IMPACT OF MUSSEL SHELL AGGREGATES ON AIR LIME MORTARS. PORE STRUCTURE AND CARBONATION

Martínez-García, Carolina[1]; González-Fonteboa, Belén[2]; Carro-López, Diego[3]; Martínez-Abella, Fernando[4]

[1]**PhD Student at the School of Civil Engineering**. Department of Construction Technology, University of A Coruña. **Postal Address**: E.T.S.I. Caminos, Canales, Puertos. Campus Elviña s/n, 15071 La Coruña, Spain. **E-mail**: carolina.martinezg@udc.es. **Telephone number**: (+34) 881015463. **Fax**: (+34) 981167170

[2]**Associate Professor at the School of Civil Engineering**. Department of Construction Technology, University of A Coruña. **Postal Address**: E.T.S.I. Caminos, Canales, Puertos. Campus Elviña s/n, 15071 La Coruña, Spain. **E-mail**: bfonteboa@udc.es. **Telephone number**: (+34) 881011442. **Fax**: (+34) 981167170

[3]**Associate Professor at the School of Civil Engineering**. Department of Construction Technology, University of A Coruña. **Postal Address**: E.T.S.I. Caminos, Canales, Puertos. Campus Elviña s/n, 15071 La Coruña, Spain. **E-mail**: dcarro@udc.es **Telephone number**: (+34) 881015429. **Fax**: (+34) 981167170

[4]**Professor at the School of Civil Engineering**. Department of Construction Technology, University of A Coruña. **Postal Address**: E.T.S.I. Caminos, Canales, Puertos. Campus Elviña s/n, 15071 La Coruña, Spain. **E-mail**: fmartinez@udc.es. **Telephone number**: (+34) 881011443. **Fax**: (+34) 981167170

Abstract

Galician "Rías"·conditions (extension, water temperature….) enable the production of excellent quality cultured mussels. This leads Spain to be the third producer country in the world. Cannery industry (35% of the total cultured mussel production) generates 25000 tons of mussel shell waste per year. Hence, it is necessary to find a sustainable use for this material. The purpose of this work is to verify the most significant changes in the properties of air lime coating mortar when replacing limestone sand with mussel shell sand. Two different air limes have been used: non-aged hydrated commercial lime powder

and 10 month-old slaked lime putty. Reference mortars and mortars with mussel shell aggregate as a substitute for limestone aggregate at different rates - 25%, 50% and 75% - have been tested. The behaviour of mortars at the age of one year from kneading has been studied. Studies show that mussel shell increases the pore volume of air lime mortar mixtures, which means a reduction in the mortar's workability and density. The poor paste-aggregate cohesion of mussel shell particles in the air lime matrix worsen the mortar mechanical strength results, which is confirmed by ultrasound test results. Carbonation at this age and hygric behaviour are properties that improve with mussel shell content.

Keywords:

Mussel shell; coating mortar; air lime; air content; microstructure; capillarity

Highlights:

- Air lime mortars with mussel shell as aggregate were designed.

- ITZ of mussel shell aggregate was compared with ITZ of a limestone aggregate.

- Chemical characteristics and shape of mussel shell affect the pore size distribution of air lime mortars.

- Mussel shell aggregate reduces capillary uptake in air lime mortars.

- Carbonation increases with mussel shell aggregate at one-year age.

1 INTRODUCTION AND OBJECTIVES

Aquaculture is the economic heart of Galicia, as it generates employment and is in constant innovation. Conditions in the Galician "Rias" enable the cultivation of excellent quality mussels, as well as extension: almost 250 thousand tonnes of mussel are produced each year, placing Spain third place in the world behind China (FAO, 2012). 35% of these mussels are transformed in the cannery industry. This produces large quantities of concentrated residue, approximately 25000 tonnes of mussel shell waste per year (Heinonen, 2014). Hence, it is of utmost importance to find a sustainable outlet for this

material, reduce the environmental impact, and avoid the shells ending up in landfills or being deposited on the seabed.

Literature includes a range of publications where seashell aggregates are used for pastes. For the most part, they study the use of oyster shell sand in cement mortar (Kuo et al., 2013; Naganathan et al., 2014; Safi et al., 2015; Wang et al., 2013; Yoon et al., 2003; Yoon, 2004). Furthermore, there are some works where cockle shells (Motamedi et al., 2015) or a mix of seashells used as aggregate in cement mortar is analysed (Liang and Wang, 2013; Nazari and Ghafouri Safarnejad, 2013). Another study uses limestone filler obtained from the calcination of mussel shells as a substitute for cement in mortar. However, the number of studies that use seashell aggregates with non-cement binders is scarce (Li et al., 2015; Liang and Wang, 2013) and only one study uses bivalve shell sand for coating mortars (Lertwattanaruk et al., 2012).

The use of different bio-waste materials to develop new by-products as well as the use of lime or cement-lime based mortars is a current trend in the construction field (Moretti et al., 2018; Nayaka et al., 2018). Therefore, in this work, the use of Galician mussel shells as aggregate in air lime coating mortars is analysed.

Building air lime has been used in construction for thousands of years as a binder (Borges et al., 2014; Ergenç and Fort-González, 2017; Jover Maestre et al., 2016; Salavessa et al., 2013). The Romans used air lime in combination with natural and artificial pozzolans in their buildings. Based on the use of this material, they were able to generate outstanding architectural and urban structures of great beauty and durability. This fact has allowed these complex systems to survive until today, maintaining much of their static, aesthetic, physical and chemical qualities. In the mid-twentieth century, air lime was relegated along with other traditional building material and systems, due to the growth in cement application, which brought about run time improvements and increases in mechanical resistance. Two generational changes were enough for the wisdom of thousands of years to be considered obsolete and the intangible heritage constituted by the knowledge of lime application, would be forgotten (Barbero-Barrera et al., 2014; Van Balen et al., 2010). Fortunately, nowadays due to concern about

environmental deterioration and the principles of sustainability, which are beginning to have a significant impact on the field of architecture, the use of lime has taken on a new dimension, displaying its technical, economic and ecological qualities. Compared with cement-based mortars, lime mortars result in a much more extended setting time, lower compressive strengths and higher porosity, deformability, and water transport characteristics (Lawrence, 2006). These last four characteristics have proven useful in the field of conservation architecture ('RILEM TC 203-RHM: Repair mortars for historic masonry', 2012) and are based on the need to develop compatible new repair materials as identified by the Venice Charter adopted by UNESCO in 1965 (Middendorf et al., 2005a, 2005b).

Traditional renders are commonly carried out in three well defined layers. According to literature, overall render performance depends on the specific function of each of its constituting layers. In this way, mortar deformability and hardness as well as water vapour permeability, water absorption by capillarity and the amount of pores should increase towards the exterior, whereas strength and pore size should decrease (Barbero-Barrera et al., 2014). All of these characteristics, as well as the mix design (binder:aggregate ratio, water content, lime characteristics, type of aggregate, etc.) influence the carbonation process, which changes the microstructure of the mortar (Santos et al., 2018), improves the mechanical properties and affects the pore structure, and hence the water transport characteristics. As it has been very well established (Cazalla et al., 2000; Cizer et al., 2012b; Lawrence et al., 2006; Mascolo et al., 2010; Nezerka, 2012; Rodriguez-Navarro et al., 1998), the carbonation reaction of lime in mortars occurs when CO_2 gas in the atmosphere dissolves into the alkaline pore solution where it reacts with $Ca(OH)_2$ leading to the precipitation of $CaCO_3$. The carbonation process is an exothermic reaction and is principally controlled by two main mechanisms: (i) diffusion of the atmospheric CO_2 gas into the pore structure of the mortar, and (ii) chemical reaction between the dissolved CO_2 and $Ca(OH)_2$. As the former is the essential step for the latter to occur through a dissolution/precipitation process, the presence of water is prerequisite for the reactants dissolution. However, water, which is present in the initial state of the mortar and released during the chemical

reaction, will hinder the CO_2 diffusion, the rate of which will depend on the pore system, drying rate, capillary transport regime and capillary condensation.

The purpose of this study was to test the use of mussel shell aggregate in traditional air lime mortars and the effects on their properties. Although it is known that the type of aggregate affects the behaviour of lime mortars (Scannell et al., 2014), studies that include recycled sand (Stefanidou et al., 2014) or variations of conventional aggregates (limestone and silicate) are scarce in number.

2   MATERIALS AND METHODS

2.1   Binders

In this work two types of air lime were used: a non-aged hydrated commercial lime powder (EN 459-1 CL90-S (AENOR, 2016)) and a slaked lime putty (EN 459-1 CL90-PL (AENOR, 2016)). Both CL 90, with 90% minimum content of calcium and magnesium oxides (AENOR, 2016). The composition of both limes is mainly calcium without any hydraulic or pozzolanic addition. In the FRX analysis (Table 1), it can be seen that apart from calcium, they present reduced quantities of magnesium, silicon, aluminate and sulphate, with a residual presence of other oxides.

Table 1. FRX composition of non-aged lime and lime putty.

Oxide (%)	LOI	CaO	MgO	SiO_2	SO_3	Al_2O_3	Fe_2O_3	K_2O	SrO	CuO	MnO	ZnO
Non-aged Lime	25.5	72.1	0.59	0.29	0.83	0.11	0.059	0.030	0.043	0.012	0.025	0.009
Lime Putty	22.6	70.5	1.40	0.93	0.41	0.26	0.13	0.042	0.029	0.011	0.005	0.009

LOI: Loss on ignition at 975˚C

Hydrated lime powder is an air lime produced by slaking quicklime with sufficient water to produce a dry powder. Lime putty is produced by slaking quicklime in an excess of water for a specific time (maturation). In this work, the lime putty was a commercial lime obtained by slaking quicklime with water and storing if for 6 months. The water content of the lime putty is 64%, similar to that indicated in others studies (Faria et al., 2008). As the lime mortars were made about 4 months after receiving the lime putty bags, it is estimated that the lime putty used in this study was 10 months old. The non-

5

aged lime powder was received, stored immediately and kept sealed until its use to avoid contact with atmospheric CO_2.

As processes used to obtain S and PL are different, they lead to different binder microstructures, which subsequently affect the final mortar properties. Upon ageing, porlandite crystals submerged in water undergo a considerable crystal size reduction, and the hexagonal crystals transform into plate-like nanometre-scale crystals, which contributes to an overall increase in surface area. These changes justify the high quality of aged high-calcium lime putties (Rodriguez-Navarro et al., 1998).

As stated by Cazalla et al. (2000), four morphologies have been identified in the aged lime putties: prismatic hexagonal crystals; tabular, plate-like crystals (most common); fibrous crystals; and nanometre-sized spherical aggregates. Non-aged hydrated lime powder shows no spherical morphologies. In addition, other authors (Margalha et al., 2013; Mascolo et al., 2010; Ruiz-Agudo and Rodriguez-Navarro, 2010) observed the same gradual change in size and shape, as prismatic hexagonal crystals started to separate into finer and smaller crystals. This crystal separation involves the progressive loss of free water. The water also tends to penetrate the crystals and propitiates the recrystallization into the plate-like structure. This transformation leads calcium hydroxide particles to become separated and remain enveloped with a strongly bound water pellicle (Cazalla et al., 2000; Cizer et al., 2012a). This may be the reason for the greater plasticity observed in limes with long slaking periods.

 In Table 2, it can be seen that lime putty presents higher specific surface area than hydrated lime.

Table 2 Characterization of non-aged hydrated lime and lime putty

		Non-aged Hydrated Lime	Lime Putty
TGA loss (%)	40-350°C	1.12	2.87
	350-600°C	21.12	21.40
	600-900°C	3.28	3.26
	Total	25.52	27.53
	$CaCO_3$ (%)[a]	7.46	7.41
	$Ca(OH)_2$ (%)[a]	86.85	88.00
	S_{BET} (m^2/g)	14.68	20.19
Density (g/cm3)		0.56	1.20 (with water)

[a] *Determined using TGA*

Transmission electron microscopy (TEM) images of both binders (hydrated and lime putty) (Fig. 1) show large micrometer-sized prismatic portlandite crystals in the non-aged hydrated lime (left), whereas smaller, nanometric (colloidal) plate-like portlandite crystals are abundant in the aged lime putty (right).
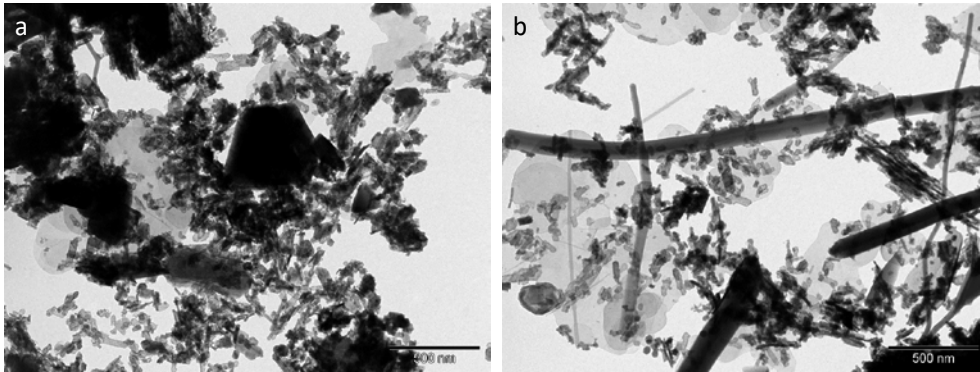
Fig. 1. Transmission electron microscopy (TEM) images: a) non-aged hydrated lime, b) lime putty.

Fig. 2 shows the XRD patterns of both S and PL, non-aged lime powder and lime putty. In general, the crystallography of both limes is similar, showing the presence of portlandite and calcite. However the lime putty sample shows a higher intensity of calcite peaks; this is congruent with the ageing of the lime putty (Cazalla et al., 2000). Another analysis is the comparison of the relative height of portlandite peaks in terms of platelet abundance (Cazalla et al., 2000; Rodriguez-Navarro et al., 1998):

$$A_{(0001)} = I_{(0001)}/I_{(10\bar{1}1)}$$

A(0001): platelet abundance; $I(0001)$: intensity at 2θ=18.1˚ and $I(10\bar{1}1)$: intensity at 2θ=34.1˚

This platelet abundance ratio was 0.52 for non-aged lime and 1.03 for lime putty. The higher proportion of the lime putty is related to the microstructural transformation during ageing (Mascolo et al., 2017). The calcium hydroxide changes from a prismatic structure to another based on hexagonal portlandite plates (Cazalla et al., 2000; Margalha et al., 2013; Rodriguez-Navarro et al., 1998). In long-term aged lime-putty this ratio is even higher and this transformation entails a higher quality of the

7

lime binder (Margalha et al., 2013; Rodriguez-Navarro et al., 1998) .This is also coherent with the TEM microscopy.
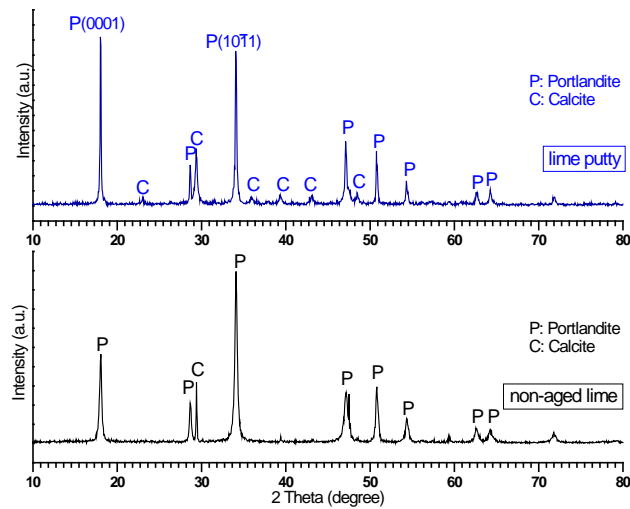
Fig. 2. XRD patterns of the lime putty and the non-aged lime.

Fig. 3 shows the TGA results of the two types of lime used. Both present a similar trend with three mass reductions. Firstly, the loss of intermolecular water, then the dihydroxylation of the calcium hydroxide and, at higher temperature, the decarbonation of the calcium carbonate.
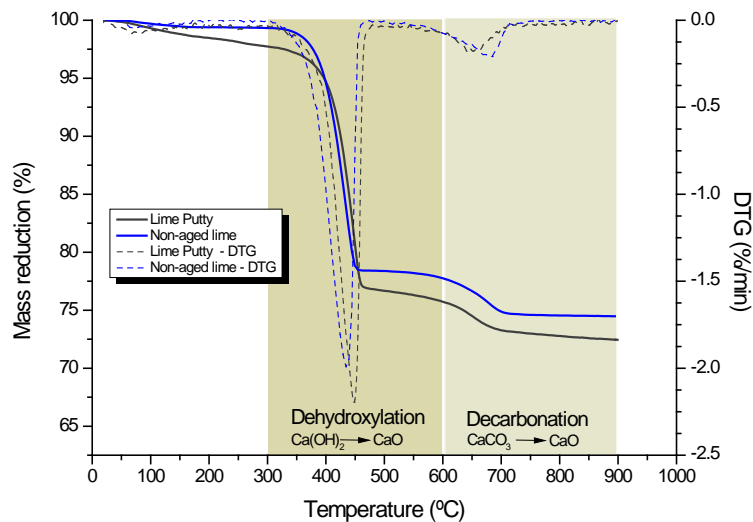
Fig. 3. TGA of non-aged lime powder and lime putty.

It is possible to calculate the percentage of hydroxide, which is both the binding and more significant fraction of this construction material. The method proposed by Margalha et al. (2013) was used for

this calculation. The assumed hypotheses are that the loss between 300 and 600 °C corresponds to dehydroxylation and that the range from 600 to 900 °C consists of only CO_2 removal. It can be seen (Table 2) that the adsorbed water is slightly higher for the lime putty. The amount of binding $Ca(OH)_2$ is similar and higher than 85% in both types of lime. Finally, the carbonated fraction of the limes is around 7.5% in both types of lime, a value similar to a lime putty of 1 year of age (Margalha et al., 2013). In the TGA curves it can be seen that the lime putty contains a higher fraction of adsorbed water, coherent with the plate-like transformation of the ageing of the lime putty (Margalha et al., 2013).
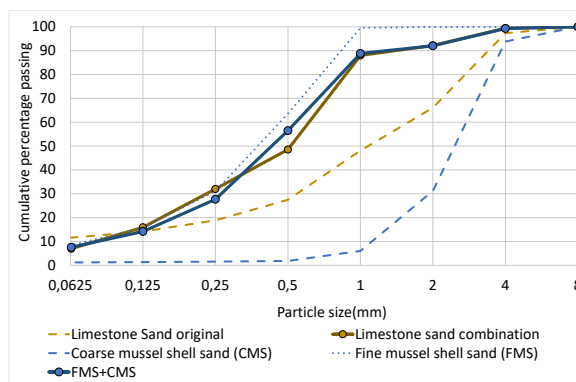
2.2 Aggregates

The limestone sand used comes from crushed limestone and it has a maximum size of 4 mm. Since its particle size distribution was not suitable for producing coating mortars, a size separation by sieving was performed (Fig. 4). Then the size fractions were combined, resulting in suitable sand with a maximum size of 2 mm (LS).

The mussel shell sand used was obtained from a heat treatment (135°C for 32 min (European Parliament and Council, 2009)). Then it was crushed and sieved. This resulted in two different size fractions: a coarse sand (CMS 0-4mm) and a fine sand (FMS 0-1mm), with a fineness modulus of 1.9 and 4.64 respectively. These two fractions were combined to obtain a mussel shell sand (MS) with an equivalent particle size distribution to the limestone sand (LS), with a fineness modulus of 3.71.

Table 3 shows the limestone and mussel shell sand properties. The mussel shell presents a small presence of chlorides, soluble sulphates and organic matter, especially the finer fraction.

According to the results of the X-ray diffraction (XRD) characterisation, mussel shells are composed mainly of calcium carbonate (95%) (Table 4). The second compound present is silicon oxide, which has a higher quantity in finer samples of the mussels. Third is the presence of sodium oxide, which can be related to the presence of sodium chloride in the samples. These results are consistent with those published by other authors (Lertwattanaruk et al., 2012; Yoon et al., 2003; Yoon, 2004).

These shells are formed by the biomineralisation of $CaCO_3$ with a small amount of organic matrix which holds the structure together (Génio et al., 2012). Mussel shells, like all bivalves, can be divided into three parts: the outer layer, periostracum, the middle layer called the prismatic layer and the inner layer referred to as nacre (Fig. 5). The periostracum is unmineralised and composed mainly of a protein. The central and thicker layer (around 400 µm) has a prismatic structure with an array of parallel calcite prisms, which are polygonal in cross section and grow from the periostracum at an angle of around 30° to the surface. The last layer, about 10 µm in width, is known as nacre which comprises laminar aragonite oriented parallel to the surface and held together with an organic matrix composite of polysaccharides (chitin), proteins and glycoproteins (Génio et al., 2012).

Fig. 4. Particle size distribution of aggregates.

Table 3. Mussel shell and limestone sand properties.

Properties	Standard	CMS (0-4mm)	FMS (0-1mm)	LS (0-4mm)
Particle density (kg/dm^3)	UNE-EN 1097-6 (AENOR, 2006a)	2.65	2.73	2.67
Water absorption (%)	UNE-EN 1097-6 (AENOR, 2006a)	2.56	4.12	2.22
Chlorides (%)	UNE-EN 1744-1 (AENOR, 2014a)	0.28	0.51	0
Soluble sulphates (%)	UNE-EN 1744-1 (AENOR, 2014a)	0.63	0.59	0
Soluble sulphates (%)	UNE-EN 1744-1 (AENOR, 2014a)	1.6	1.3	-
Organic matter (%)	UNE 103-204-93 (AENOR, 1993)	1.49	2.15	-
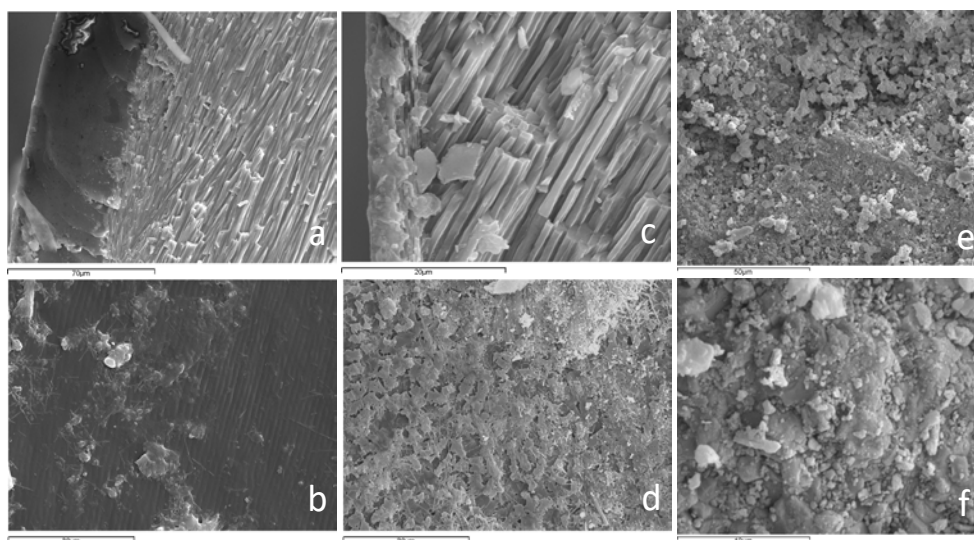
Fig. 5. SEM analysis of mussel shell composition: a) Periostracum (external layer) - prismatic structure layer; b) Periostracum layer front view; c) Prismatic structure layer – Nacre layer; d) Nacre layer front view; e and f) limestone particle.

Table 4. CMS and FMS chemical composition. *Stoichiometrically calculated.

%	CMS	FMS
$CaCO_3$*	95.088	94.664
SiO_2	1.112	2.580
Na_2O	0.354	0.508
Al_2O_3	< 0.01	< 0.01
SO_3	0.176	0.308
MgO	0.205	0.277
Fe_2O_3	< 0.005	< 0.005
SrO	0.116	0.192
K_2O	< 0.006	< 0.006
P_2O_5	0.087	0.105
Cl	< 0.009	< 0.009
Br	0.009	0.012
ZnO	< 0.004	< 0.004
CuO	0.010	0.011
ZrO_2	0.005	0.010
LOI 550˚C	4.058	4.280
LOI 975˚C	44.208	42.108

2.3 Mortar Mixes

Two series of mortars, one with lime putty and the other with lime powder, were designed as a reference. Each series was modified replacing, by volume, the limestone sand with mussel shell sand. The substitution rates used were 25%, 50% and 75%. Substitution percentage of 100% was discarded

in a preliminary test as the consistency of the mix was too stiff or harsh. Table 5 shows the basic mix parameters of both series.

Thus, a water/lime ratio of 1.7 (by volume) was used to design the mortars with non-aged hydrated lime powder.

In accordance to literature (Lanas and Alvarez, 2003) a suitable binder to aggregate ratio could be 1:3 (by volume). However, it is known that mussel shell aggregates increases water demand in mixtures. Thus, in this work the binder/aggregate ratio used for both lime putty mortars and non-aged lime mortars was in the range of 1:2.5 to 1:2.3 (by volume).

As a result, eight types of air lime mortars were obtained, four with non-aged lime powder: SL0, SL25, SL50 and SL75 and another four with lime putty: PL0, PL25, PL50 and PL75. Table 5 shows the mix proportions by weight of both the reference and mussel shell mortars and also shows paste:aggregate and water:lime ratios used in the mixes.

Table 5. Air lime mortars dosages by weight.

|		Mass per litre of mortar (g)			
	Substitution rate (%)	0	25	50	75
PL	Lime putty	629.09	629.09	629.09	629.09
	Added water	0	0	0	0
	Limestone Sand (LS)	1270.28	952.71	635.14	317.57
	Mussel shell sand (MS)	0	323.52	647.03	970.55
	Paste: Aggregate	0.5			
	Water: Lime	1.77			
S	Non-aged lime powder	207.39	207.39	207.39	207.39
	Added water	357.95	357.95	357.95	357.95
	Limestone Sand (LS)	1468.17	1101.12	734.08	367.04
	Mussel shell sand (MS)	0	373.91	747.83	1121.74
	Paste: Aggregate	0.39			
	Water: Lime	1.73			

2.4 Test methods

2.4.1 Mixing and moulding

After chemical and physical characterization of binders and aggregates, the raw materials were mixed in order to obtain the different mortars.

The mixing procedure was developed according to UNE-EN 196-1 (AENOR, 2005): firstly, lime putty or water and hydrated lime powder were blended for 30 seconds at low speed. Then the aggregate was added and mixed for 30 seconds at low speed and 30 seconds at high speed. The mixing procedure was then stopped for 90 seconds, the mixer walls were scrapped in the first 30 seconds and finally, mixing continued for 60 seconds at high speed. Different batches were made to determine the fresh state and hardened state behaviour of each mortar.

For hardened state tests, mortars were cast in prismatic moulds (40x40x160 mm). The moulding process was done according to UNE-EN 1015-11 (AENOR, 2007). Moulds (without the bottom) were placed on a glass plate covered with two layers of white cotton gauze. Then mortars were cast in two layers. A manual compaction system with a 50 g rammer was used to remove air bubbles (Fig. 6). After that, two layers of white cotton gauze, six layers of absorbent filter paper and a glass plate were placed (in this sequence) on the fresh mortar. After that, moulds were turned upside down, and the glass plate, now sited on the top, was removed carefully and the cotton gauze was covered with six layers of absorbent filter paper. The mould was returned to its original position and a load of 5 kg was applied during 3 hours. After these 3 hours, all the absorbent filter papers and gauzes were removed and moulds were introduced in the climatic chamber (20 °C ± 2 and 60 ± 5%) for 5 days before demoulding. The CO_2 concentration in the chamber was estimated to be the standard atmospheric concentration (i.e. 0.033 ± 0.001% by volume).

Prismatic samples (40x40x160 mm) were used to measure hardened density, carbonation front by phenolphthalein test, compressive strength (AENOR, 2007) and water absorption by capillarity action UNE-EN 1015-18 (AENOR, 2003).
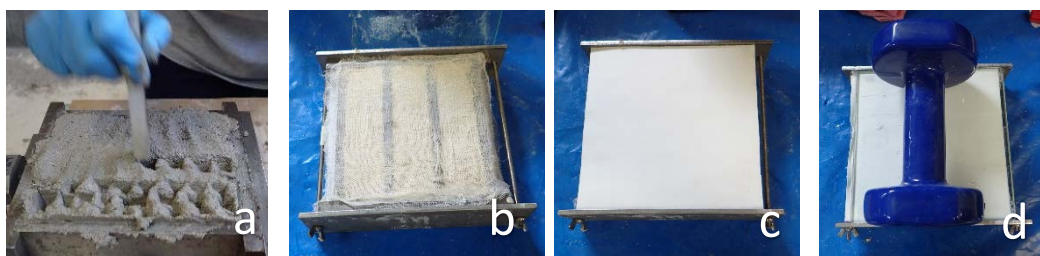
Fig. 6. Casting procedure: a) second mortar layer compacted with 25 bumps with a 50 g rammer; b) mortar with two layers of white cotton gauze; c) six layers of absorbent filter paper placed on the gauze; d) mould turned upside down with gauzes, filter papers, the glass plate loaded with a 5 kg-load.

2.4.2   Fresh state

In fresh state, air content and consistency were determined just after mixing. Air content was developed according to UNE-EN 413-2 (AENOR, 2006b) . Consistency was measured using the flow table method and the penetration probe method, according to UNE-EN 413-2 (AENOR, 2006b).

The fresh density is calculated as the fresh mass of the mortar divided by the volume of the filled mould, using the average mass of all batches made.

2.4.3   Microstructure: Optical and electronic microscopy

Mortar samples were pre-consolidated by impregnation with resin under vacuum. Thin sections were cut and polished to the thickness of approximately 20 microns, covered with a glass slip and examined with LEICA DM750M optical microscopy. Specimens used for scanning electron microscopy (SEM) were dehydrated and covered with gold in a Bal-Tec SCD 004 sputter coater. Then they were examined and photographed under a JEOL JSM-6400 Scanning Electron Microscope.

2.4.4   Porosity, pore distribution and water absorption

By means of a core-drill, at least three pieces were taken from different samples of hardened lime mortars at the age of 1 year. They were used to measure water absorption and accessible porosity for water according to UNE 83980 (AENOR, 2014b). In addition, the pore size distribution was performed with a Mercury Intrusion Porosimetry (MIP), which automatically registers pressure, pore diameter in a range between 0.003 to 200 µm, intrusion volume, and pore surface area. The range of pressure used was 6.29 KPa to 410759.65 KPa.

The water absorption by capillarity test was determined according to UNE-EN 1015-18 (AENOR, 2003). Three 160x40x40 mm samples of each mortar were used for this test. After drying to constant mass,

the four largest faces of the test pieces were sealed using paraffin, and then these test pieces were broken (under a flexural test) in two halves. The test pieces were placed on the tray with the broken faces of the prisms turned down on four metal cylinder supports so that they did not touch the bottom of the tray, and were immersed in water to a height of 5 to 10 mm for the duration of the test. The specimens were removed from the container after 10 minutes, the surface water quickly removed with a damp cloth, and the specimens were weighed (M1) and removed immediately from the container. The same procedure was repeated after 90 minutes and weighed (M2). The capillary absorption coefficient is calculated using the following expression: C= 0.1 (M2-M1) kg/(m^2.min$^{0.5}$).

2.4.5   Carbonation

The carbonation evolution over time was detected by impregnating the mortar samples with a saturated phenolphthalein ethyl alcohol solution. Phenolphthalein is a chemical compound that turns colourless in acidic or near neutral solutions (pH < 8.2). It starts to be visible at pH of about 8.2 and changes colour completely at pH of about 9.8.

Three test samples of each mortar were tested. Each sample of 16x4x4cm was broken at 365 days. After a few seconds, phenolphthalein was sprayed on broken mortar surfaces. Then, photographs were taken to follow-up the evolution of the colouration produced on the surface of the samples treated with phenolphthalein. This follow-up was done a few seconds, several minutes, several hours and a day after the spray. This photographic monitoring was carried out to ensure the development of the colouration caused by phenolphthalein in the different lime mortars. Photographic images (Fig. 7) were scanned and digitally analysed using processing software (Image-j), where the percentage of the carbonated surface can be measured on the total area of the treated sample.
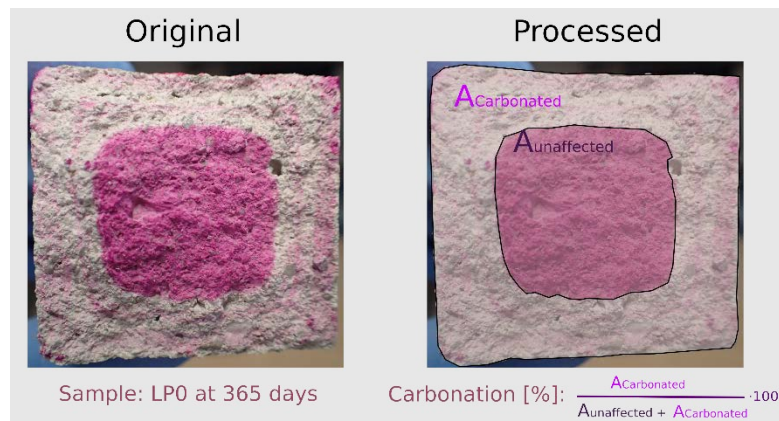
Fig. 7. Measurement of the different coloured areas of samples treated with phenolphthalein spray solution, to determine the carbonation development over time in air lime mortars.

2.4.6 Compressive strength and ultrasonic wave propagation

The compressive test was carried out on prismatic specimens 160x40x40 mm using a universal multi-purpose touch-screen compression/flexural MATEST S205N Unitronic 50 KN with Cyber-Plus evolution control. Specimens were tested according to UNE EN 1015-11 (AENOR, 2007). The test velocity selected for flexural strength was 0.02 KN/s and for compressive strength was 0.15 KN/s.

Ultrasonic measurement equipment, Pundit Lab from Proceq, was used to perform the ultrasonic test in transmission reception mode. The frequency of both transducer couples was 150 Hz. Two measurements were made on each prismatic specimen, on a section of 40x40 mm, at the width and depth of the tested piece. Three specimens were used for each mortar, thus six speeds for each type of mortar were registered.

3 RESULTS AND DISCUSSION

Different tests methods were developed and results were analysed. Standard deviation was calculated and the values obtained were in the range of other authors results (Faria et al., 2008). Materials were provided in a single lot and they were kept in laboratory conditions during all the testing period. All tests were developed in a fixed time period (so that temperature is not affecting results) by a single operator. These conditions guarantee a good repeatability, so that, standard deviations are low.

16

3.1 Consistency

Fig. 8 and Fig. 9 show spread diameter and penetration depth results, values that are related to mortar consistency. It can be seen that workability is reduced with the incorporation of mussel shell aggregate. Mussel shell mortars present lower spread diameter and lower penetration depth than baseline mortars. The mussel particle shape (with a high percentage of flaky particles) significantly increases water demand, which increases mortar consistency. This fact combined with the water absorption capacity (Table 3) of the aggregate (higher than that of the limestone aggregate), leads to a reduction in mussel shell mortar workability.

Moreover, as aforementioned in section 2.1, slaking lime with water leads to an ageing process that produces continuous changes in the morphology of portlandite crystals. These changes involve a crystal shape transformation and also a size reduction (from micrometer to sub-micrometer or nanometre). Both these issues change mortar rheology (Cazalla et al., 2000; Mascolo et al., 2010; Rodriguez-Navarro et al., 1998). In addition non-aged mortars incorporate higher quantities of aggregates (b:agg=0.39) than lime putty mortars (b:agg=0.50). Despite all these issues non-aged mortars present lower consistencies than lime putty mortars. According to Margalha (2013) this can be due to the of chemically unbound or free water content that is higher in non-aged lime mortars than in lime putty mortars.

Lastly, it appears that the penetration test is more sensitive than the flow table test to the incorporation of mussel shell (Fig. 6). The reduction of the penetration depth obtained with S75 mortar is 61% while this percentage is 24% when calculated with the spread diameter. Accordingly, the results got with PL75 show the same trend, reductions of 35% and 15% are obtained with the penetration test and the table test respectively. This higher sensitivity may be attributed to the procedure carried out with the penetration test where the mussel shell flaky particles act strongly as obstacles to the probe penetration (Martínez-García et al., 2017).
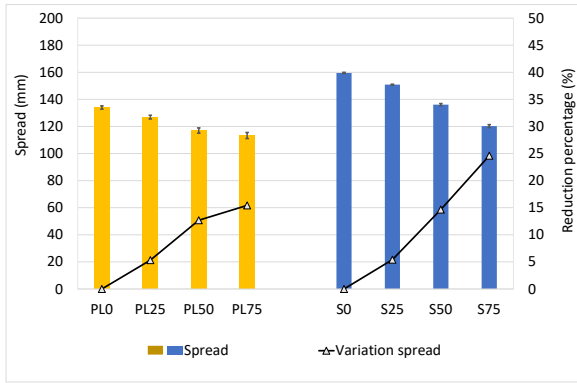
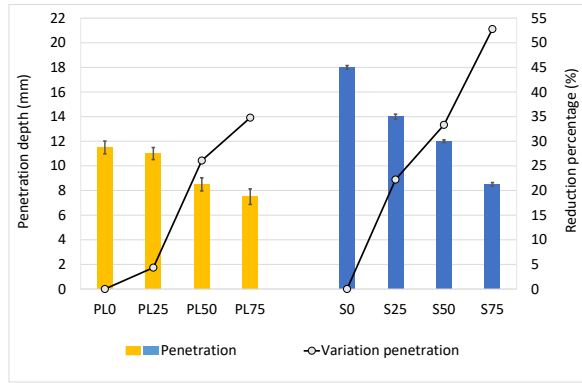**Fig. 8. Spread diameter of air lime mortars.**

Fig. 9. Penetration depth of air lime mortars.

3.2 Density and air content

Fresh and hardened (365 days) density values of all mortars are shown in Fig. 10. The results show that lime putty and non-aged hydrated mortars present similar fresh and hardened density values.

On the other hand, density decreases with the mussel shell content. The decrease shows the same trend in fresh and hardened state regardless of the binder type analysed. In hardened state both PL75 and S75 show a density reduction of approximately 10%, when compared to the baseline mortars PL0 and S0 respectively. In fresh state, density drops are slightly higher in hydrated lime mortars than in lime putty ones. In this case, compared to the baseline mortars, PL75 and S75 show a fresh density reduction of 5% and 6% respectively.

Fig. 11 shows air content of air lime mortars. In agreement with density results, the air content increases with the incorporation of mussel shell aggregate.

This effect (density reductions and air content increment) is attributed to irregular and flaky mussel shell particles. The sand particle shape affects the amount of entrapped air in the mortar. The more asymmetrical the particles, the larger amount of air in the mortars. In addition, one of the main components of mussel shell is chitin, an organic protein which is a kind of polysaccharide that produces air (Centauro et al., 2017; Martínez-García et al., 2017). There is a clear relationship between the organic matter content, and the density or air content of the mortars (Fig. 12 and Fig. 13)
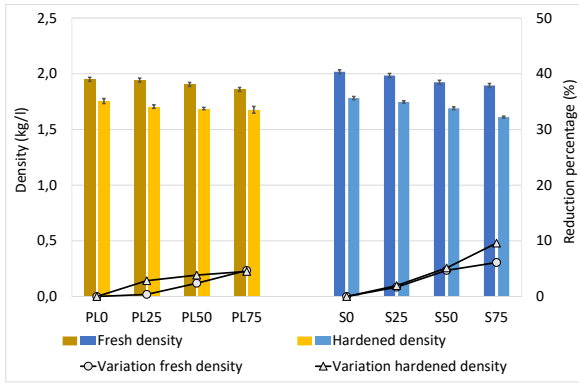
18

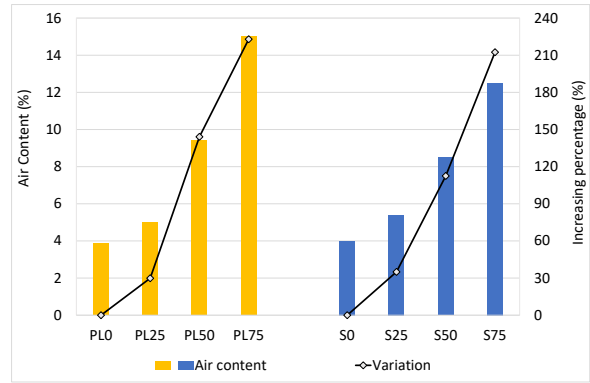**Fig. 10. Fresh and hardened mortar density.**
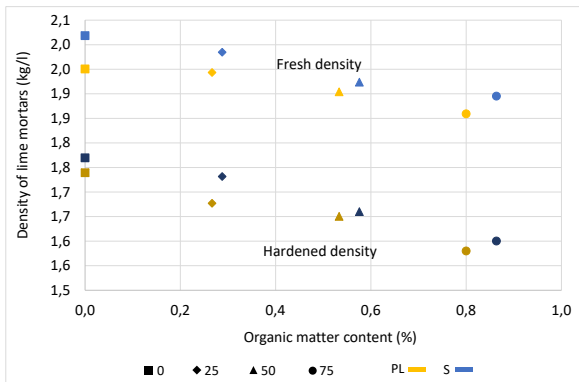

Fig. 11. Air content.

Fig. 12. Relationship between density and organic matter content.
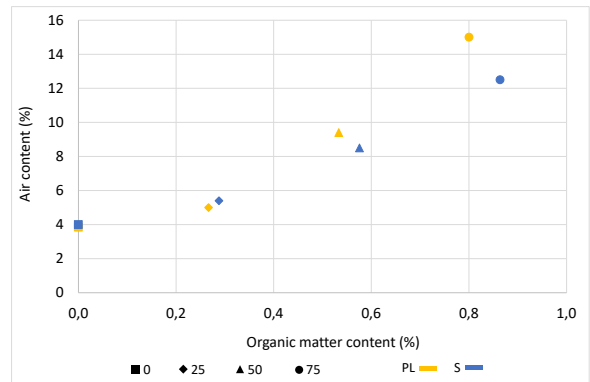

Fig. 13. Relationship between air content and organic matter content.

3.3 Microstructure

Optical-microscope microphotographs (Fig. 14) and SEM images (Fig. 15) show lime putty and non-aged hydrated lime mortars with different mussel shell content (0%, 25%, 50% and 75%) at 365 days. The images show the differences in matrix and interfacial transition zone (ITZ) as a function of the mussel shell percentage.

Optical images show coarse pores in lime mortars with high mussel shell content (especially PL75 and S75). These coarse pores are greater than 100 µm in diameter and usually they are formed by entrapped or entrained air. Entrapped air pores are generated by the entrapment of air during mixing. They present both irregular shape and distribution. On the contrary, entrained air pores are round

voids formed by organic materials containing proteins. In this case, air pores shown in the images present both irregular and bubble-like shapes, which means they were produced by entrapped air due to the mussel particle shape, as well as the organic protein present in the mussel shell (Centauro et al., 2017). Reference mortars (PL0 and S0) hardly show this kind of porosity. In general, non-aged lime mortars show a slightly greater quantity of coarse pores than lime putty mortars due to a higher aggregate content in the mixture.

Accordingly, SEM images show greater porosity in mussel shell mortars than in reference mortars. Furthermore, with these SEM images the different ITZs can be properly seen. Special attention has to be paid to the ITZ between the lime-based matrix and mussel particles which is assumed to have a significant influence on the mortar's mechanical performance.

The limestone aggregate used in reference mortars is a crushed sand with a rough texture that improves mechanical bonding with the lime matrix. Therefore, the interfacial transition zone of reference mortars is not a separate region but a gradual transition from the aggregate surface into the paste. This can be observed in both PL0 and S0 mortars. On the contrary, mussel aggregate particles are smooth and flat which leads to decreased bonding with the air lime matrix. Hence, clear high porosity is shown in the ITZs of mussel shell mortars. In addition, all mussel mortars present a matrix phase with small cracks in the vicinity of the mussel shells where micro-cracks are formed due to the irregular shape of the aggregate.
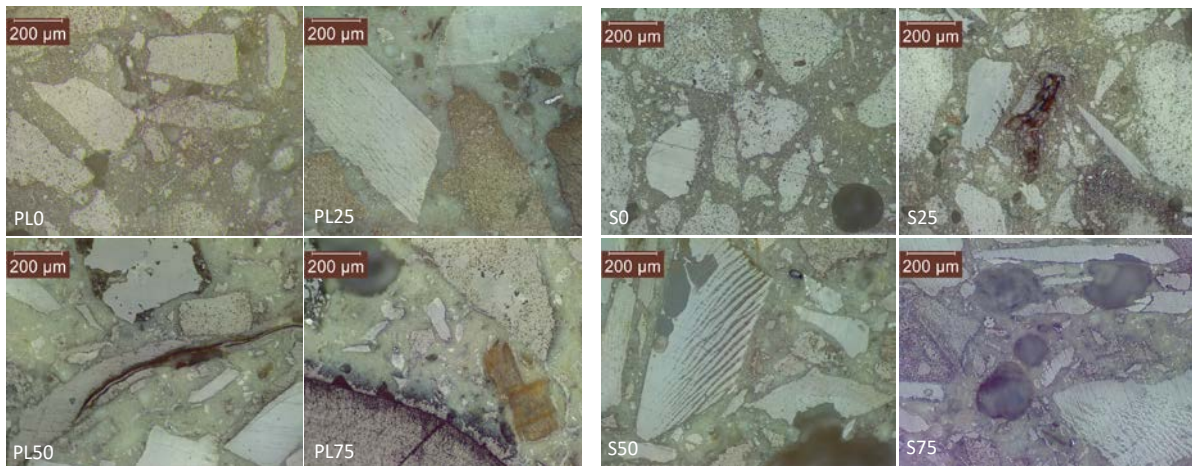
Fig. 14. Optical-microscope microphotographs of lime putty and non-aged lime mortars at 365 days.
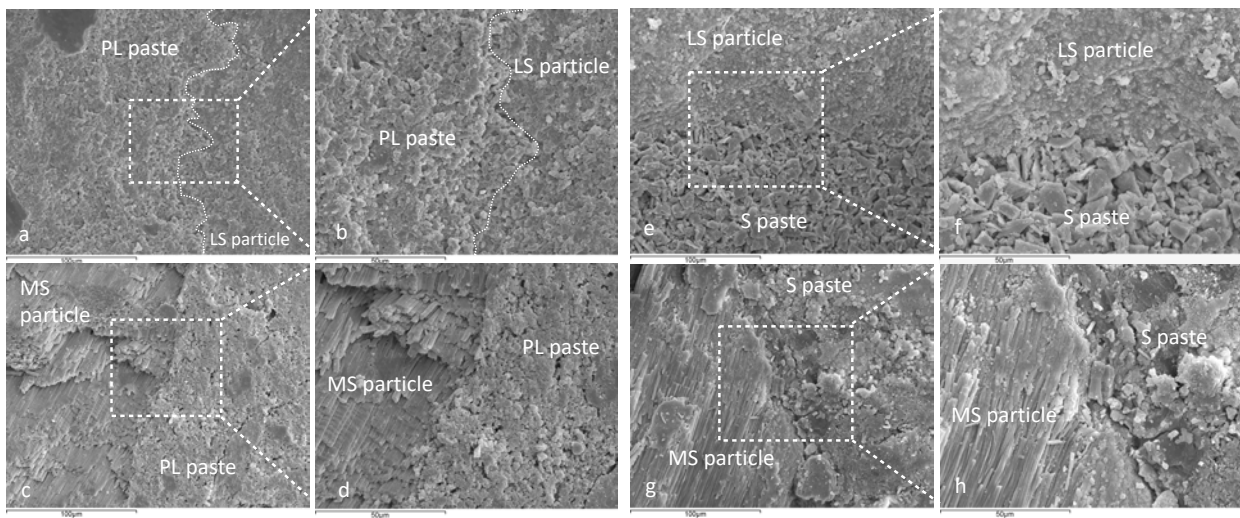
Fig. 15. SEM images of air lime mortars at 365 days: PL0 (a, b); PL75 (c, d); S0 (e, f) and S75 (g, h).

3.4 Pore size distribution

Pore size distribution of all mortar was measured with MIP and all analysed samples used in this test (between 0.5-0.8 cm^3) showed a similar open porosity value (PL: 29 ± 2%, S: 25 ± 2%). The pore size distribution is presented in Fig. 16.

As also observed by other authors (Arandigoyen et al., 2005; Arizzi and Cultrone, 2013, 2012; Lanas and Alvarez, 2003; Lawrence et al., 2007; Rodriguez-Navarro et al., 2002) in this work, all mortars (lime putty and non-aged mortars) showed a bimodal distribution with two peaks, one related to medium

sized pores (between 0.1 and 1 μm in diameter-structural peak) and the other to large sized pores (5–30 μm, depending on the mortar type-ITZ peak).

However, the pore size distribution of the mussel shell mortars with high mussel percentages is clearly distinct from that of mortars with low mussel aggregate content. Regarding structural peak, mortars with 75% and 50% mussel shell aggregate present a considerably lower peak value than mortars without mussel shell content or with only 25%. This can be seen in both lime putty and non-aged mortars, and especially in the latter.

Analysing ITZ peak, it is seen that as the mussel shell content increases, the percentage of pores between 5 and 40 μm considerably increases. This effect can again be seen in both non-aged and lime putty mortars.

Finally, mussel shell aggregate content increases the volume of large pores (>50 μm), which is more noteworthy in non-aged lime mortars than in lime putty ones. A notable trend of a shift in the pore size distribution to higher values is observed with the use of mussel shell aggregate.

Most of the measured pores are between 0.1 and 100 μm, so they are interconnected capillary pores that contribute to water and air transfer through capillary action (Nunes and Slížková, 2014; Silva et al., 2015). Sorption pores (<0.1 μm) are gel pores that develop in hydrated phases. In lime-based mortars, pores smaller than 0.1 μm are in limited amounts as they are related to the presence of hydraulic phases as CSH. These pores are formed inside the crystals. Finally coarser pores, above 100 μm, are formed due to entrapped or entrained air as aforementioned.

Small capillary pores (<1 μm) are formed in the binder matrix when water evaporates. Arandigoyen et al. (2005) studies that the main peak (0.5-1 μm) varies according to kneading water used in mortar preparation: the more kneading water used the bigger the volume of pores in this peak due to evaporation. As all mussel shell mortars were prepared with the same water as their corresponding baseline mortar, the lower volume of pores in the main peak in these mortars is due to the fact that flaky particles might create a barrier for water evaporation. Moreover, S0 and S25 present a similar quantity of small capillary pores as PL0 and PL25. However, S50 and S75 show a lower volume of these

pores than PL50 and PL75 respectively because the S mix composition incorporates a higher aggregate content than the PL mix. Therefore, when mussel shell is used at a high percentage, its barrier effect leads to a significant decrease in small capillary pores.

Large capillary pores, sometimes considered as those over 50 μm (Lanas and Alvarez, 2003), sometimes as those over 4-50 μm (Arizzi and Cultrone, 2012) are formed in the spaces between the binder and the aggregate. They occur when the aggregate shape results in bad cohesion between the binder and the aggregate, leading, in addition, to strength reductions. All mussel shell mortars present a higher volume of large capillary pores, which agrees with the microstructure observations that showed a clear high porosity in the ITZs of mussel shell mortars. Also in accordance with microstructure images, S mortars (with more aggregate content) present a higher quantity of these large pores.

Finally, the presence of mussel shell does not affect the sorption pores (<0.1 μm), their quantity being similar regardless of the mussel shell content.
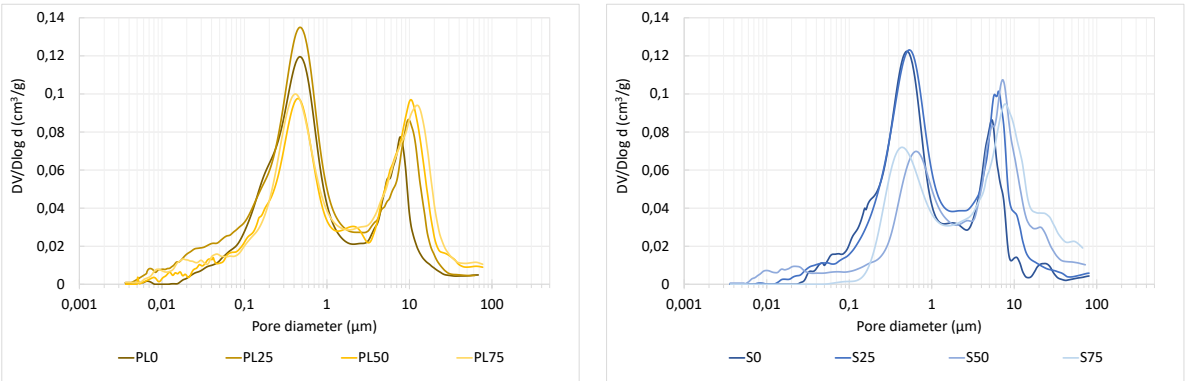
Fig. 16. Pore size distribution using MIP.
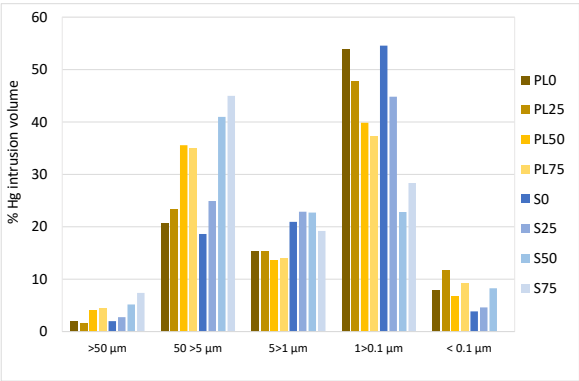
Fig. 17. Pore size ranges of air lime mortars.

3.5 Porosity and water absorption

The open water-accessible porosity and the water absorption of all mortars are shown in Fig. 18 and Fig. 19 respectively. Regarding water absorption, both water absorption after immersion, and water absorption after immersion and boiling are shown. As expected, the latter is greater than the former because simple absorption in water does not result in the complete saturation of a porous material as air remains in the pores. Introducing the same saturated samples in boiling water leads to the pore structure being penetrated more fully.

According to these tests, all mussel shell mortars present greater porosity and water absorption than their corresponding baseline mortars. Compared with the baseline mortars, PL75 and S75 show a porosity increment of 28% and 20% respectively and water absorption increases again of 26% and 21% respectively.

Comparing these results to the ones obtained with MIP, it is observed that the porosity of mortars with 0% and 25% obtained with MIP, is higher than the porosity measured with water penetration. However, the opposite trend is detected when analysing mortars with 50% and 75% mussel shell. In general, the values of porosity obtained with MIP are higher than those measured with water penetration (Arandigoyen et al., 2005) because higher pressure is used with mercury. However, according to aforementioned results, mussel shell mortars with high replacement percentages present a significantly high air content (Fig. 11). Therefore, these mortars show the presence of isolated pores with large radii (exceeding 200 µm) due to air entrainment or entrapment. This pore size radius is not present in the MIP distribution curves and, in addition, as these pores may be isolated mercury cannot enter.
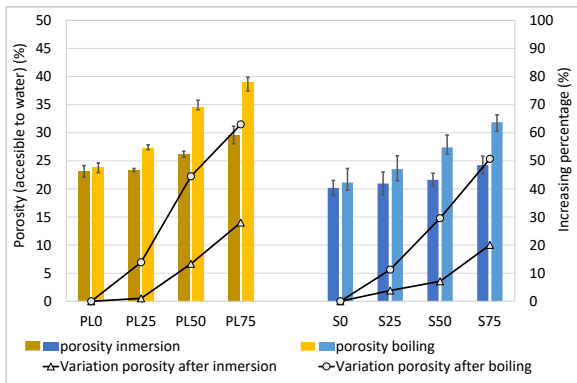
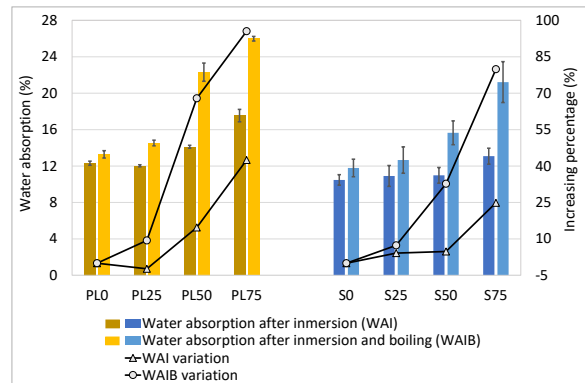**Fig. 18. Porosity accessible to water.**

Fig. 19. Water absorption.

3.6 Water absorption by capillarity

Water absorption by capillarity of air lime mortars at 365 days was calculated according to UNE EN 1015-18 (AENOR, 2003) using results obtained at 10 min and 90 min (Fig. 20). However, to compare with the results obtained by other authors (Faria et al., 2008; Faria and Martins, 2013) the capillarity curves (from 0 min to 90 min) are presented in Fig. 21. The slope between 0 and 10 min is similar to the slope between 10 and 90 min, which guarantees that the curve is not yet in the asymptotic area. Therefore, the values obtained with 10 minutes and 90 minutes can be used to calculate the capillary coefficient (Fig. 20).

The results show that PL0 presents a similar (slightly higher) capillary coefficient to S0. In addition, the mussel shell content significantly decreases the value of water absorption by capillarity. In lime putty mortars, the reduction is in the range of 30 to 40% for all mussel mortars. Non-aged hydrated lime mortars show greater reduction percentages, 36%, 53% and 69% for S25, S50 and S75 respectively.

Capillarity is a phenomenon resulting from the competition between adsorption forces of the polar solid surface and cohesive forces between the water molecules. If the adsorption forces of the material surface are high enough, water can rise even against gravity. Then capillarity may be affected by: contact angle that the liquid makes on a solid surface, capillary pore radius, pore shape, and connectivity (Centauro et al., 2017).

Arizzi and Cultrone (2013) suggests that pores with a radius between 0.1 and 1 μm have the greatest influence on capillary uptake, i.e. the higher the volume of pores in this range the lower the capillarity. Therefore, at the same open total porosity, the capillary coefficient is expected to be higher in pastes with a smaller pore diameter (Rodriguez-Navarro et al., 2002) due to the fact that capillary force increases as pore diameter decreases. According to the experimental results discussed in previous sections, PL0 mortar presents a higher volume of pores with diameter < 1μm than S0, which justifies its slightly higher capillary coefficient. In addition, S mortar was made with a slightly higher aggregate content than lime putty mortar, which also contributes to PL being more susceptible to water uptake by capillarity (Arizzi et al., 2013).

Regarding the effect of mussel shell, all mussel shell mortars present a higher volume of large capillarity pores and also greater isolated pores with a large radius (exceeding 200 μm) due to the entrapment and entrainment air (in this last case, these pores may also present low connectivity).

Besides, according to pore size distribution, S50 and S75 show a smaller volume of small pores than PL50 and PL75 respectively. Therefore, the reduction in the capillary coefficient is more significant in S mortars than in PL mortars.

Finally, it is also presumable that the elongated shape of the mussel shell particles could be blocking the capillary rise of water. In addition, as was previously discussed, mussel shell particles present an organic protein (chitin) that may develop certain hydrophobic behaviour leading to a reduction in the water contact angle and hence, the water absorption by capillarity.
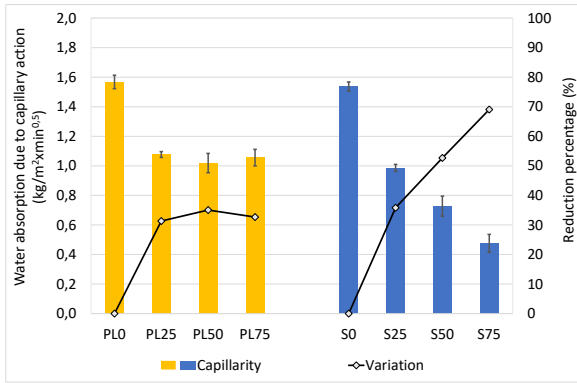
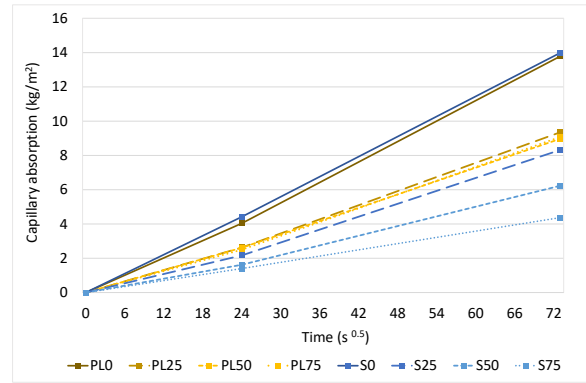Fig. 20. Water absorption coefficient due to capillary action.

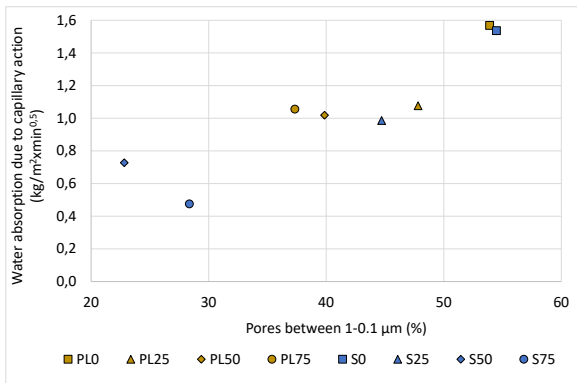Fig. 21. Capillary water absorption curves (0-90min)

Fig. 22. Water absorption due to capillary action versus porosity between 0.1 – 1 µm.

3.7 Carbonation

The carbonation front was measured by spraying a freshly broken surface of mortars with phenolphthalein at 365 days (Fig. 23). This coloured area was measured in three samples of each mortar and, using digital analysis, an average value of the percentage of the carbonated area was calculated (Fig. 24). The percentage was determined from photographs taken 20 minutes after being sprayed with the phenolphthalein solution.

Fig. 24 shows that at 365 days the mussel shell content increases the carbonation area of air lime mortars. Analysing lime putty mortars it is observed that the percentage of carbonation in PL25, PL50 and PL75 is 0.5, 16 and 26.3% higher than that measured in PL0, respectively. Non-aged lime mortars also show increments of 1.9, 5.9 and 5.3%, corresponding to S25, S50 and S75 respectively.

Finally, agreeing with Cazalla et al. (2000), lime putty mortars (in this study with less than 1 year of ageing) and non-aged lime mortars present a similar carbonation degree at the age of one year.

The pore structure and the pore water content play an important role in the progress of carbonation in lime mortars by controlling the rate of CO_2 diffusion and the reactants' dissolution and concentration, as well as the pore solution supersaturation (Cizer et al., 2012a; Mosquera et al., 2002). In summary, carbonation reaction in lime mortars is only sustained if a free path exists for CO_2 gas to move into the mortar and if water is present at the same time for the reactants to dissolve (Lawrence, 2006; Mosquera et al., 2002).

Regarding water content, it is well known that the amount of water is critical for the carbonation reaction, as it is needed for dissolution of calcium hydroxide and CO_2, although an excess of water will block the pore system. In fact, the optimum water content for carbonation is that corresponding to maximum adsorption on the surface of the pores before capillary condensation. To get to this stage, a prior drying process takes place. The drying process presents two phases, a first drying phase that consist of drying at the surface and capillary water transported to the surface, and then a second drying phase that is developed by the diffusion of water to the surface. In the first phase, carbonation hardly exists because carbon dioxide is not allowed to diffuse into the pores (Cizer et al., 2012b, 2012a; Hendrickx et al., 2010).

In this regard, water absorption by capillarity is lower in mussel shell mortars than in baseline mortars. This means that the water exchange capacity between the interior of the paste and the exterior is low. Therefore, although it is probable that the carbonation rate will be lower in mussel shell mortar than in baseline mortar, at one year of age, the available water content is going to be higher in the former than in the latter. This water content allows carbonation to significantly develop at one year of age and justifies that mussel shell mortars present, at 365 days of age, a higher carbonation area than reference mortars.

On the other hand, once carbonation is initiated, it develops in different phases: (i) diffusion of gaseous CO_2 through the open pores, (ii) dissolution of $Ca(OH)_2$ in the pore water releasing Ca^{2+} and OH^- ions,

(iii) absorption and dissolution of CO_2 in the alkaline pore water forming carbonic acid (H2CO3), (iv) its dissociation as bicarbonate (HCO^{3-}) and carbonate (CO_3^{2-}) ions, and (v) reaction between Ca^{2+} and CO_3^{2-} ions forming $CaCO_3$ through nucleation and subsequent crystal growth (Moorehead, 1986).

Regarding CO_2 diffusion, Rodriguez-Navarro (2002) states that porosimetry plots of carbonated pastes tend to be at the right side of non-carbonated pastes curves, i.e. the pore size and pore volume is greater. Actually, according to Lawrence et al. (2007), pores larger than 10 μm offer the greatest access to atmospheric CO_2, affecting the carbonation process. This trend agrees with the curves shown by the mussel shell mortars. These curves show that mussel shell aggregate increases porosity and redistributes the pore structure (Fig. 16). Air lime mortars with mussel shell aggregate show a greater volume of pores larger than 10 μm, which allows greater access to the diffusion of CO_2. Therefore, in these mortars atmospheric CO_2 easily penetrates into paste, which again demonstrates their higher carbonation area compared to the area shown by reference mortars.

Also Fig. 23 shows that reference mortars, both PL0 and S0, present Liesegang patterns or rings (Cazalla et al., 2000; Lawrence et al., 2006; Rodriguez-Navarro et al., 2002), which are also more defined in non-aged lime mortar (they can be already seen 1 minute after spraying) than in lime putty mortar (detected only 5 minutes after spraying). Furthermore, mussel shell mortars do not show these Liesegang patterns.

The Liesegang phenomenon is quasi-periodic and self-organized, occurring in the wake of a moving reaction front (García-Ruiz et al., 1996; Oliveira et al., 2017). The development of Liesegang patterns in the carbonating of lime mortars is explained as follows: $Ca(OH)_2$ is dissolved in the water condensed in the mortar pore system (as Ca^{2+}). CO_2 diffuses and also dissolves as CO_2^{-3} in the water. CO_2^{-3} readily reacts with Ca^{2+} and forms a colloid-size calcium carbonate, which will be followed by spontaneous nuclei growth and precipitation if the local concentration reaches a nucleation threshold. This threshold represents the energy barrier for the transition of the calcium carbonate from the molecular state to solid state. The wake of the moving reaction front toward the sample core finally results in the described alternating $CaCO_3^-$ rich and $Ca(OH)_2^-$ rich rings. Liesegang patterns develop when a high

volume of pores with r<0.1 µm are presented. These small pores can sustain very high supersaturation ratios with respect to $CaCO_3$, resulting in higher nucleation rates, a crucial fact for pattern development due to the Laplace effect of curvature (Rodriguez-Navarro et al., 2002). Therefore, as mussel shell aggregate mortars do not have a high volume of small pores, they do not encourage any scenario for the formation of Liesegang patterns. Furthermore, water migration in mussel shell mortars is difficult, which leads to low supersaturation ratios, which result in limited calcite precipitation. In this case, carbonation occurs in a closer-to-equilibrium diffusion-limited system with no Liesegang patterns. However, this complex phenomenon requires further research, analysing carbonation at early ages.
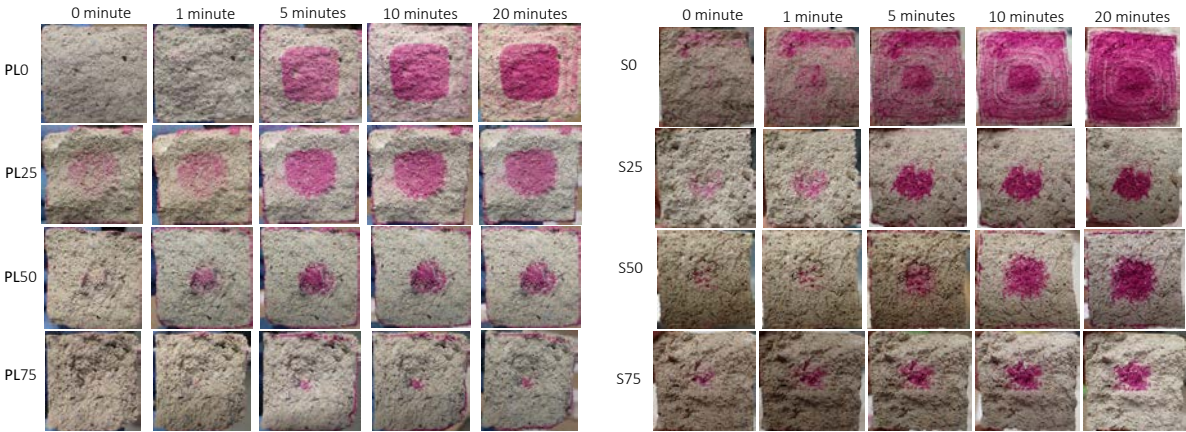
Fig. 23. Appearance of freshly broken faces of 365 days carbonate lime putty (left) and non-aged hydrated lime (right) mortars samples treated with phenolphthalein at 0, 1, 5, 10 and 20 minutes after being sprayed.
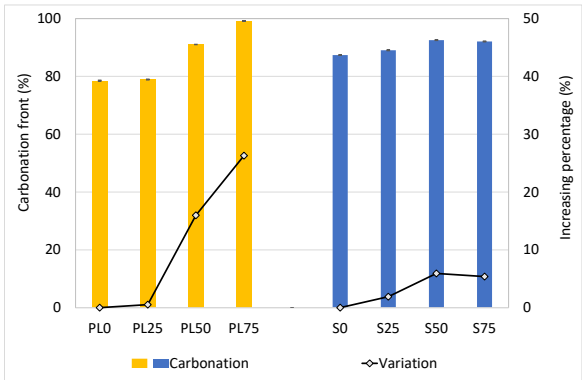
Fig. 24. Carbonation front of lime putty mortars and non-aged hydrate lime at 365 days.

3.8 Mechanical properties and ultrasonic wave propagation

Results of compressive strength at 365 days are shown in Fig. 25. From these results it can be concluded that lime putty mortars present slightly higher compressive strengths than non-aged mortars. In addition, the mussel shell content significantly decreases this mechanical property. In PL75 and S75 the reductions are 17.70% and 9.12% respectively.

According to previous discussion, porosity is higher in mussel shell mortars with high mussel content. As discussed, the irregular and flaky particle shape of the mussel sand, and its organic matter content, introduce a large volume of large pores. In addition, the smooth mussel shell surface develops a weak ITZ with the air lime matrix. All these issues justify the significant compressive strength reductions detected in the mussel shell mortars.

As is well known, the carbonation process positively affects the mortar's mechanical properties. The carbonation process changes the porous system of the mortar due to water evaporation (Arizzi et al., 2013). In addition, it produces a porosity decrease which results in an increase in mechanical strength and compactness (Arizzi et al., 2013). It has been reported that when portlandite transforms into calcite an increase in the solid volume of about 12% takes place (Cazalla et al., 2000). As was detected, at 365 days, carbonation front of mussel shell mortars is higher than in baseline mortars. Although the carbonation area is higher in mussel mortars than in baseline mortars, this does not compensate for the effect of the higher porosity and weak ITZ of these mortars.
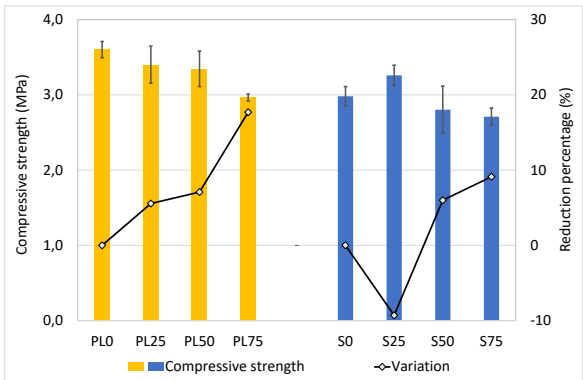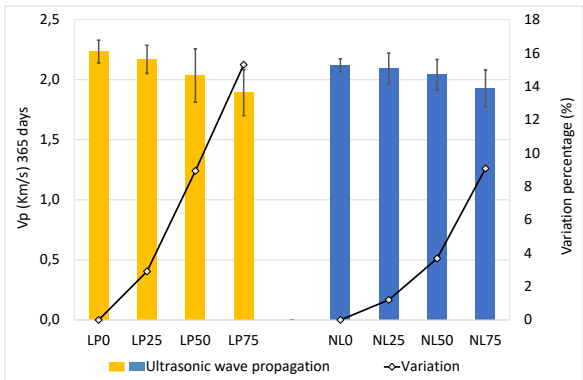

Fig. 25. Compressive strength (MPa).　　　**Fig. 26. Ultrasonic wave propagation (Km/s).**

Results of ultrasonic test measured at 365 days are shown in Fig. 26. In accordance with compressive strength results, baseline lime putty mortars present similar ultrasonic velocities to non-aged mortars. Moreover, mussel shell aggregate reduces the ultrasonic wave velocity in all air lime mortars. This reduction is more noticeable in lime putty mortars than in non-aged lime mortars, at 10% in S75 while this percentage is about 25% in PL75.

Lime mortar is a two-phase material consisting of an aggregate enclosed by a porous matrix. In each phase the ultrasonic wave propagation is different, depending on the final velocity, the volume of each material and the particular wave velocity throughout the matrix and throughout the aggregate. Pore volume, pore size or crystal size of both matrix and aggregate are some of the main parameters influencing wave propagation. In this regard, Arizzi et al. (2013) asserts that the two main parameters influencing ultrasonic wave propagation are the matrix porosity and carbonation degree. Regarding the carbonation degree, a reduction in porosity in the mortar matrix is associated with this process and, in addition, the density, modulus of elasticity and Poisson coefficient are higher in calcite than in portlandite (Schön, 1998; Speziale et al., 2008). Therefore, the ultrasonic velocity is expected to be higher in mortars with a larger carbonation front.

In this work, the carbonation front in the mussel shell mortars is larger than in the baseline mortar, although they present a significantly high porosity in the ITZs and the matrix because of air pores generated by entrapped air due to the mussel particle shape and the organic protein present in the shells. This high porosity has a prevalent effect on both the compressive strength and ultrasonic velocity, leading to a considerable decrease in wave propagation velocity when mussel particles are used (Fig. 27).
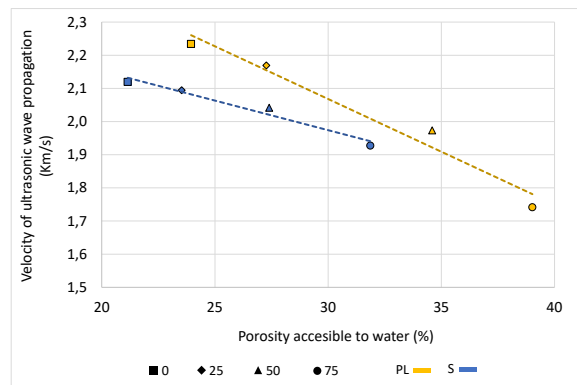
Fig. 27. Porosity accessible to water versus ultrasound test.

3.9 Technical feasibility and environmental overview

The industry of cultured or wild mussels encompasses more than 40 countries. The potential use of the waste generated in this industry will overcame the expensive and problematic issues of waste disposal. In addition, the use of a waste to design new construction bio-products will promote the sustainability of this field.

One of the main requirements in the development of the recycled product was that the process to obtain it had to be a low environmental impact process. Hence, the heat treatment carried out to obtain the seashell aggregate was low temperature and short duration, and it was not necessary to consume water for its processing. Whit this process, a mussel shell aggregate was obtained. In the same line of sustainability, this new aggregate was employed in lime based mortars.

The mortar characteristics that are affected to a lower extent with the incorporation of mussel shell aggregate are those related to mechanical properties. This can be seen with the results obtained in compressive strength or ultrasound wave propagation. Therefore, when 25% replacement percentage of mussel shell is used the reductions in these properties are always lower than 6%.

Properties related to porosity and pore size distribution, that is, air content, water absorption and capillarity are more sensitive to the mussel incorporation. Porosity rises significantly; on the other hand, capillarity drops sharply. Therefore, durability should be analysed in further research to

determine accurately the behaviour of mussel shell mortars in the long term. In any case, when 25% replacement percentage is used, porosity increase is 14%, which seems to indicate that durability of these mortars is guaranteed.

Finally, it was seen that the mussel shell incorporation affects mortar with slaked lime putty to a similar extent than mortar with non-aged hydrated lime.

4 CONCLUSIONS

This work studies the use of mussel shell aggregate as a substitute for limestone sand in coating mortars with two air lime binders: a non-aged hydrated commercial lime powder (S) and a 10-month slaked lime putty (PL). Different replacement rates of limestone aggregate with mussel shell aggregate (25%, 50% and 75%) were used, so a total of 8 mixtures were studied, including the reference mortar (without mussel shell): S0, S25, S50, S75, PL0, PL25, PL50 and PL75. The results obtained allowed the following conclusions to be drawn:

The mussel aggregates present a particle shape with a high percentage of flaky particles, which leads to a significantly increased water demand and, hence, affects the mortar consistency.

In addition, the mussel shell shape attached to the organic matter content (due to the organic protein, chitin) introduces both irregular and bubble-like voids and changes the pore size distribution in mussel mortar.

Firstly, mussel shell aggregate leads mortar to present a higher volume of large capillarity pores (exceeding 50 μm) and also greater isolated pores with large radii (exceeding 200 μm). This leads to increased water absorption in mussel shell mortar. Moreover, these pores occur when the aggregate shape results in poor cohesion between the binder and the aggregate (large and porous ITZ), leading, in addition, to strength reductions. Furthermore, the presence of these large pores guarantees the entry of higher volume of CO_2, which affects the carbonation degree.

Lastly, mussel shell aggregate characteristics reduce the volume of pores in the structural peak (0.1-1 µm) which leads to a reduction in the capillary coefficient. This reduction has to be combined with the effect of elongated particles blocking the capillary rise of water. Both these issues indicate that the water exchange capacity between the interior of the paste and the exterior is low. Therefore, at one-year of age, the available water content is going to be higher in mussel shell mortars. This fact combined with the entry of a higher volume of CO_2 justifies the higher carbonation degree of mussel mortars at an age of 1 year.

After the results analysis it can be confirm that the replacement percentage of 25% of conventional sand by mussel shell sand leads to obtain a lime based mortar with suitable characteristics to be use as base-layer coating and as surface-layer coating. A mussel shell aggregate was obtained with a low environmental process and a low impact binder was used. The use of the mussel coating designed in this work will contribute to move construction field towards sustainability.

ACKNOWLEDGEMENT

REFERENCES

AENOR, 2016. UNE-EN 459-1, Building lime. Part 1: Definitions, specifications and conformity criteria.

AENOR, 2014a. UNE-EN 1744-1,Tests for chemical properties of aggregates. Part 1: Chemical analysis.

AENOR, 2014b. UNE 83980, Concrete durability. Test methods. Determination of the water absorption,

density and accessible porosity for water in concrete.

AENOR, 2007. UNE-EN 1015-11, Methods of test for mortar for masonry. Part 11: Determination of flexural and compressive strength of hardened mortar.

AENOR, 2006a. UNE-EN 1097-6, Tests for mechanical and physical properties of aggregates. Part 6: Determination of particle density and water absorption.

AENOR, 2006b. UNE-EN 413-2, Masonry cement. Part 2: Test methods.

AENOR, 2005. UNE-EN 196-1, Methods of testing cement. Part 1: Determination of strength. Méthodes.

AENOR, 2003. UNE-EN 1015-18, Methods of test for mortar for masonry. Part 18: Determination of water absorption coefficient due to capillary action of hardened mortar.

AENOR, 1993. UNE 103204, Organic matter content of a soil by the potassium permanganate method.

Arandigoyen, M., Bernal, J.L.P., López, M.A.B., Alvarez, J.I., 2005. Lime-pastes with different kneading water: Pore structure and capillary porosity. Appl. Surf. Sci. 252, 1449–1459. https://doi.org/10.1016/j.apsusc.2005.02.145

Arizzi, A., Cultrone, G., 2013. The influence of aggregate texture, morphology and grading on the carbonation of non-hydraulic (aerial) lime-based mortars. Q. J. Eng. Geol. Hydrogeol. 46, 507–520. https://doi.org/10.1144/qjegh2012-017

Arizzi, A., Cultrone, G., 2012. The difference in behaviour between calcitic and dolomitic lime mortars set under dry conditions: The relationship between textural and physical-mechanical properties. Cem. Concr. Res. 42, 818–826. https://doi.org/https://doi.org/10.1016/j.cemconres.2012.03.008

Arizzi, A., Martínez-Martínez, J., Cultrone, G., 2013. Ultrasonic wave propagation through lime mortars: an alternative and non-destructive tool for textural characterization. Mater. Struct. 46, 1321–1335. https://doi.org/10.1617/s11527-012-9976-1

Barbero-Barrera, M., Maldonado-Ramos, L., Van Balen, K., García-Santos, A., Neila-González, F.J., 2014.

Lime render layers: An overview of their properties. J. Cult. Herit. 15, 326–330. https://doi.org/10.1016/j.culher.2013.07.004

Borges, C., Santos Silva, A., Veiga, M.R., 2014. Durability of ancient lime mortars in humid environment. Constr. Build. Mater. 66, 606–620. https://doi.org/10.1016/j.conbuildmat.2014.05.019

Cazalla, O., Rodriguez-Navarro, C., Sebastian, E., Cultrone, G., De la Torre, M.J., 2000. Aging of lime putty: Effects on traditional lime mortar carbonation. J. Am. Ceram. Soc. 83, 1070–1076. https://doi.org/10.1111/j.1151-2916.2000.tb01332.x

Centauro, I., Cantisani, E., Grandin, C., Salvini, A., Vettori, S., 2017. The influence of natural organic materials on the properties of traditional lime-based mortars. Int. J. Archit. Herit. 11, 670–684. https://doi.org/10.1080/15583058.2017.1287978

Cizer, Ö., Rodriguez-Navarro, C., Ruiz-Agudo, E., Elsen, J., Van Gemert, D., Van Balen, K., 2012a. Phase and morphology evolution of calcium carbonate precipitated by carbonation of hydrated lime. J. Mater. Sci. 47, 6151–6165. https://doi.org/10.1007/s10853-012-6535-7

Cizer, Ö., Van Balen, K., Elsen, J., Van Gemert, D., 2012b. Real-time investigation of reaction rate and mineral phase modifications of lime carbonation. Constr. Build. Mater. 35, 741–751. https://doi.org/10.1016/j.conbuildmat.2012.04.036

Ergenç, D., Fort-González, R., 2017. Preliminary investigation of the preparation of repair mortars for the Temple Of Diana, Mérida, Spain. Ge-Conservacion 1, 42–49.

European Parliament and Council, 2009. Regulation (EC) No 1069/2009. Off. J. Eur. Union 300, 1–33.

FAO, 2012. The European market for mussels.

Faria, P., Henriques, F., Rato, V., 2008. Comparative evaluation of lime mortars for architectural conservation. J. Cult. Herit. 9, 338–346. https://doi.org/10.1016/J.CULHER.2008.03.003

Faria, P., Martins, A., 2013. Influence of Air Lime type and Curing Conditions on Lime and Lime-Metakaolin Mortars, in: Freitas, V.; Delgado, J. (Ed.), Durability of Building Materials and

Components. Building Pahology and Rehabilitation. Springer, Berlin, Heidelberg, pp. 105–126. https://doi.org/10.1007/978-3-642-37475-3_5

García-Ruiz, J.M., Rondön, D., Garcia-Romero, A., Otâlora, F., 1996. Role of gravity in the formation of liesegang patterns. J. Phys. Chem. 100, 8854–8860.

Génio, L., Kiel, S., Cunha, M.R., Grahame, J., Little, C.T.S., 2012. Shell microstructures of mussels (Bivalvia: Mytilidae: Bathymodiolinae) from deep-sea chemosynthetic sites: Do they have a phylogenetic significance? Deep. Res. Part I Oceanogr. Res. Pap. 64. https://doi.org/10.1016/j.dsr.2012.02.002

Heinonen, K., 2014. Farmed Mussels Report. Monterey Bay Aquarium's Seafood Watch®, p. 56.

Hendrickx, R., Roels, S., Van Balen, K., 2010. Measuring the water capacity and transfer properties of fresh mortar. Cem. Concr. Res. 40, 1650–1655. https://doi.org/10.1016/J.CEMCONRES.2010.08.002

Jover Maestre, F.J., Pastor Quiles, M., Martínez Mira, I., Vilaplana Ortego, E., 2016. El uso de la cal en la construcción durante la Prehistoria reciente: nuevas aportaciones para el levante de la Península Ibérica. Arqueol. la Arquit. 13, 5–10. https://doi.org/http://dx.doi.org/10.3989/arq.arqt.2016.005

Kuo, W. Ten, Wang, H.Y., Shu, C.Y., Su, D.S., 2013. Engineering properties of controlled low-strength materials containing waste oyster shells. Constr. Build. Mater. 46, 128–133. https://doi.org/10.1016/j.conbuildmat.2013.04.020

Lanas, J., Alvarez, J.I., 2003. Masonry repair lime-based mortars: Factors affecting the mechanical behavior. Cem. Concr. Res. 33, 1867–1876. https://doi.org/10.1016/S0008-8846(03)00210-2

Lawrence, R.M., Mays, T.J., Rigby, S.P., Walker, P., D'Ayala, D., 2007. Effects of carbonation on the pore structure of non-hydraulic lime mortars. Cem. Concr. Res. 37, 1059–1069. https://doi.org/10.1016/j.cemconres.2007.04.011

Lawrence, R.M.H., 2006. A study of carbonation in non-hydraulic lime mortars. PhD Thesis 344.

Lawrence, R.M.H., Mays, T.J., Walker, P., D'Ayala, D., 2006. Determination of carbonation profiles in non-hydraulic lime mortars using thermogravimetric analysis. Thermochim. Acta 444, 179–189. https://doi.org/10.1016/j.tca.2006.03.002

Lertwattanaruk, P., Makul, N., Siripattarapravat, C., 2012. Utilization of ground waste seashells in cement mortars for masonry and plastering. J. Environ. Manage. 111, 133–141. https://doi.org/10.1016/j.jenvman.2012.06.032

Li, G., Xu, X., Chen, E., Fan, J., Xiong, G., 2015. Properties of cement-based bricks with oyster-shells ash. J. Clean. Prod. 91, 279–287. https://doi.org/10.1016/j.jclepro.2014.12.023

Liang, C.F., Wang, H.Y., 2013. Feasibility of pulverized oyster shell as a cementing material. Adv. Mater. Sci. Eng. 2013. https://doi.org/10.1155/2013/809247

Margalha, M.G., Silva, A.S., Veiga, M.R., de Brito, J., Ball, R.J., Allen, G.C., 2013. Microstructural Changes of Lime Putty during Aging. J. Mater. Civ. Eng. 25, 1524–1532. https://doi.org/10.1061/(ASCE)MT.1943-5533.0000687

Martínez-García, C., González-Fonteboa, B., Martínez-Abella, F., Carro- López, D., 2017. Performance of mussel shell as aggregate in plain concrete. Constr. Build. Mater. 139, 570–583. https://doi.org/10.1016/j.conbuildmat.2016.09.091

Mascolo, G., Mascolo, M.C., Vitale, A., Marino, O., 2010. Microstructure evolution of lime putty upon aging. J. Cryst. Growth 312, 2363–2368. https://doi.org/10.1016/j.jcrysgro.2010.05.020

Mascolo, M.C., Daniele, V., Mascolo, G., 2017. An approach for a rapid determination of the aging time of lime putty. Thermochim. Acta 648, 75–78. https://doi.org/10.1016/j.tca.2016.12.012

Middendorf, B., Hughes, J.J., Callebaut, K., Baronio, G., Papayianni, I., 2005a. Investigative methods for the characterisation of historic mortars---Part 1: Mineralogical characterisation. Mater. Struct. 38, 771–780. https://doi.org/10.1007/BF02479290

Middendorf, B., Hughes, J.J., Callebaut, K., Baronio, G., Papayianni, I., 2005b. Investigative methods for the characterisation of historic mortars - Part 2: Chemical characterisation. Mater. Des. 38, 771–780. https://doi.org/10.1617/14282

Moorehead, D.R., 1986. Cementation by the carbonation of hydrated lime. Cem. Concr. Res. 16, 700–708. https://doi.org/10.1016/0008-8846(86)90044-X

Moretti, J.P., Sales, A., Quarcioni, V.A., Silva, D.C.B., Oliveira, M.C.B., Pinto, N.S., Ramos, L.W.S.L., 2018. Pore size distribution of mortars produced with agroindustrial waste. J. Clean. Prod. 187, 473–484. https://doi.org/10.1016/J.JCLEPRO.2018.03.219

Mosquera, M.J., Benítez, D., Perry, S.H., 2002. Pore structure in mortars applied on restoration: Effect on properties relevant to decay of granite buildings. Cem. Concr. Res. 32, 1883–1888. https://doi.org/10.1016/S0008-8846(02)00887-6

Motamedi, S., Shamshirband, S., Hashim, R., Petković, D., Roy, C., 2015. Estimating unconfined compressive strength of cockle shell-cement-sand mixtures using soft computing methodologies. Eng. Struct. 98, 49–58. https://doi.org/10.1016/j.engstruct.2015.03.070

Naganathan, S., Silvadanan, S., Chung, T.Y., Nicolasselvam, M.F., Thiruchelvam, S., 2014. Use of Wastes in Developing Mortar – A Review. Adv. Mater. Res. 935, 146–150. https://doi.org/10.4028/www.scientific.net/AMR.935.146

Nayaka, R.R., Alengaram, U.J., Jumaat, M.Z., Yusoff, S.B., Alnahhal, M.F., 2018. High volume cement replacement by environmental friendly industrial by-product palm oil clinker powder in cement – lime masonry mortar. J. Clean. Prod. 190, 272–284. https://doi.org/10.1016/J.JCLEPRO.2018.03.291

Nazari, A., Ghafouri Safarnejad, M., 2013. Prediction early age compressive strength of OPC-based geopolymers with different alkali activators and seashell powder by gene expression programming. Ceram. Int. 39, 1433–1442. https://doi.org/10.1016/j.ceramint.2012.07.086

Nezerka, V., 2012. Microstructure, Chemical Processes and Experimental Investigation of Lime-Based

Mortars. p. 26.

Nunes, C., Slížková, Z., 2014. Hydrophobic lime based mortars with linseed oil: Characterization and durability assessment. Cem. Concr. Res. 61–62, 28–39. https://doi.org/10.1016/J.CEMCONRES.2014.03.011

Oliveira, M.A., Azenha, M., Lourenço, P.B., Meneghini, A., Guimarães, E.T., Castro, F., Soares, D., 2017. Experimental analysis of the carbonation and humidity diffusion processes in aerial lime mortar. Constr. Build. Mater. 148, 38–48. https://doi.org/10.1016/j.conbuildmat.2017.04.120

RILEM TC 203-RHM: Repair mortars for historic masonry, 2012. . Mater. Struct. 45, 1287–1294. https://doi.org/10.1617/s11527-012-9847-9

Rodriguez-Navarro, C., Cazalla, O., Elert, K., Sebastian, E., 2002. Liesegang pattern development in carbonating traditional lime mortars. Proc. R. Soc. A Math. Phys. Eng. Sci. 458, 2261–2273. https://doi.org/10.1098/rspa.2002.0975

Rodriguez-Navarro, C., Hansen, E., Ginell, William, S., 1998. Calcium Hydroxide Crystal Evolution upon Aging of Lime Putty. J. Am. Ceram. Soc. 81, 3032–3034. https://doi.org/10.1111/j.1151-2916.1998.tb02735.x

Ruiz-Agudo, E., Rodriguez-Navarro, C., 2010. Microstructure and rheology of lime putty. Langmuir 26, 3868–3877. https://doi.org/10.1021/la903430z

Safi, B., Saidi, M., Daoui, A., Bellal, A., Mechekak, A., Toumi, K., 2015. The use of seashells as a fine aggregate (by sand substitution) in self-compacting mortar (SCM). Constr. Build. Mater. 78, 430–438. https://doi.org/10.1016/j.conbuildmat.2015.01.009

Salavessa, E., Jalali, S., Sousa, L.M.O., Fernandes, L., Duarte, A.M., 2013. Historical plasterwork techniques inspire new formulations. Constr. Build. Mater. 48, 858–867. https://doi.org/10.1016/j.conbuildmat.2013.07.064

Santos, A.R., Veiga, M. do R., Santos Silva, A., de Brito, J., Álvarez, J.I., 2018. Evolution of the

microstructure of lime based mortars and influence on the mechanical behaviour: The role of the aggregates. Constr. Build. Mater. 187, 907–922. https://doi.org/10.1016/J.CONBUILDMAT.2018.07.223

Scannell, S., Lawrence, M., Walker, P., 2014. Impact of aggregate type on air lime mortar properties. Energy Procedia 62, 81–90. https://doi.org/10.1016/j.egypro.2014.12.369

Schön, J., 1998. Physical properties of rocks; fundamentals and principles of petrophysics, Handbook of geophysical exploration. Pergamon.

Silva, B.A., Ferreira Pinto, A.P., Gomes, A., 2015. Natural hydraulic lime versus cement for blended lime mortars for restoration works. Constr. Build. Mater. 94, 346–360. https://doi.org/10.1016/J.CONBUILDMAT.2015.06.058

Speziale, S., Reichmann, H.J., Schilling, F.R., Wenk, H.R., Monteiro, P.J.M., 2008. Determination of the elastic constants of portlandite by Brillouin spectroscopy. Cem. Concr. Res. 38, 1148–1153. https://doi.org/10.1016/J.CEMCONRES.2008.05.006

Stefanidou, M., Anastasiou, E., Georgiadis Filikas, K., 2014. Recycled sand in lime-based mortars. Waste Manag. 34, 2595–2602. https://doi.org/10.1016/j.wasman.2014.09.005

Van Balen, K., Bicer-Simsir, B., Binda, L., Bläuer, C., Elsen, J., Groot, C., Hansen, E., Van Hees, R., Henriques, F., Hughes, J., Toumbakari, E.E., Von Konow, T., Lindqvist, J.E., Maurenbrecher, P., Middendorf, B., Papayianni, I., Simon, S., Stefanidou, M., Subercaseaux, M., Tedeschi, C., Thomson, M., Valek, J., Valluzi, M.R., Vanhellemont, Y., Veiga, M.R., 2010. Performance and Repair Requirements for Renders and Plasters, in: 2nd Historic Mortars Conference HMC2010 and RILEM TC 203-RHM Final Workshop. Prague, Czech Republic, pp. 1359–1363.

Wang, H.Y., Kuo, W. Ten, Lin, C.C., Po-Yo, C., 2013. Study of the material properties of fly ash added to oyster cement mortar. Constr. Build. Mater. 41, 532–537. https://doi.org/10.1016/j.conbuildmat.2012.11.021

Yoon, G., Kim, B., Kim, B., Han, S., 2003. Chemical – mechanical characteristics of crushed oyster-shell.

Waste Manag. 23, 825–834.

Yoon, H., 2004. Oyster Shell as Substitute for Aggregate in Mortar. Waste Manag. Res. 22, 158–170.

https://doi.org/10.1177/0734242X04042456